JOURNAL OF MAGNETIC RESONANCE IMAGING 36:286–304 (2012)

Review: MR Physics for Clinicians

Non-Contrast Enhanced MR Angiography: Physical Principles

CME

Andrew J. Wheaton, PhD and Mitsue Miyazaki, PhD*

This article is accredited as a journal-based CME activity. If you wish to receive credit for this activity, please refer to the website: www.wileyhealthylearning.com

ACCREDITATION AND DESIGNATION STATEMENT

Blackwell Futura Media Services designates this journal-based CME activity for a maximum of 1 *AMA PRA Category 1 Credit*™. Physicians should only claim credit commensurate with the extent of their participation in the activity.

Blackwell Futura Media Services is accredited by the Accreditation Council for Continuing Medical Education to provide continuing medical education for physicians.

EDUCATIONAL OBJECTIVES

Upon completion of this educational activity, participants will be better able to discuss the primary applications, advantages, and limitations of established and emerging NCE-MRA techniques.

ACTIVITY DISCLOSURES

No commercial support has been accepted related to the development or publication of this activity.

Faculty Disclosures:

The following contributors have no conflicts of interest to disclose:

Editor-in-Chief: C. Leon Partain, MD, PhD

CME Editor: Scott B. Reeder, MD, PhD

CME Committee: Scott Nagle, MD, PhD, Pratik Mukherjee, MD, PhD, Shreyas Vasanawala, MD, PhD, Bonnie Joe, MD, PhD, Tim Leiner, MD, PhD, Sabine Weckbach, MD, Frank Korosec, PhD

Authors: Andrew J. Wheaton, PhD, Mitsue Miyazaki, PhD

This manuscript underwent peer review in line with the standards of editorial integrity and publication ethics maintained by *Journal of Magnetic Resonance Imaging*. The peer reviewers have no relevant financial relationships. The peer review process for *Journal of Magnetic Resonance Imaging* is double-blinded. As such, the identities of the reviewers are not disclosed in line with the standard accepted practices of medical journal peer review.

Conflicts of interest have been identified and resolved in accordance with Blackwell Futura Media Services's Policy on Activity Disclosure and Conflict of Interest. No relevant financial relationships exist for any individual in control of the content and therefore there were no conflicts to resolve.

INSTRUCTIONS ON RECEIVING CREDIT

For information on applicability and acceptance of CME credit for this activity, please consult your professional licensing board.

This activity is designed to be completed within an hour; physicians should claim only those credits that reflect the time actually spent in the activity. To successfully earn credit, participants must complete the activity during the valid credit period.

Follow these steps to earn credit:

- Log on to www.wileyhealthylearning.com
- Read the target audience, educational objectives, and activity disclosures.
- Read the article in print or online format.
- Reflect on the article.
- Access the CME Exam, and choose the best answer to each question.
- Complete the required evaluation component of the activity.

This activity will be available for CME credit for twelve months following its publication date. At that time, it will be reviewed and potentially updated and extended for an additional period.

Toshiba Medical Research Institute, Vernon Hills, Illinois, USA.
*Address reprint requests to: M.M., Toshiba Medical Research Institute, 706 N. Deerpath Dr., Vernon Hills, IL 60061.
E-mail: mmiyazaki@tmriusa.com
Received July 14, 2011; Accepted February 15, 2012.
DOI 10.1002/jmri.23641
View this article online at wileyonlinelibrary.com.

Noncontrast-enhanced magnetic resonance angiography (NCE-MRA) methods have been demonstrated in anatomies throughout the body. Previously established NCE-MRA techniques suffered from long scan times or low sensitivity. Advances in hardware and software have made NCE-MRA scan times clinically feasible. Recent concerns over the safety of gadolinium-based contrast material combined with the expense of the material and its administration have generated a demand for NCE-MRA. In response, several new NCE-MRA methods have been developed. The physical mechanisms underlying five general classes of NCE-MRA methods (inflow effect, flow-dependency on cardiac phase, flow-encoding, spin labeling, and relaxation) are explained. The original techniques of time-of-flight (TOF) and phase contrast MRA (PC-MRA) are briefly introduced. New developments in NCE-MRA, including hybrid of opposite-contrast (HOP-MRA), four dimensional PC-MRA (4D Flow), cardiac-gated 3D fast-spin-echo, flow-sensitive dephasing (FSD), arterial spin labeling (ASL), and balanced steady-state free-precession (bSSFP) are highlighted. The primary applications, advantages, and limitations of established and emerging NCE-MRA techniques are discussed.

Key Words: angiography; noncontrast; unenhanced; MRA
J. Magn. Reson. Imaging 2012;36:286–304.

MAGNETIC RESONANCE ANGIOGRAPHY (MRA) applications have been a general application of MRI practice since the inception of clinical MRI. The first applications of MRA were performed without exogenous contrast enhancement. These techniques leveraged the MR-related differences between flowing and stationary spins to generate depictions of bright vessels on a dark background. These techniques, including time-of-flight (TOF) and phase contrast (PC), were the earliest developments of noncontrast-enhanced MRA (NCE-MRA).

The use of gadolinium-based contrast enhancement for MRA (CE-MRA), introduced in 1994 (1), greatly accentuated the signal from inflowing blood via the T1-shortening effect of gadolinium, resulting in improved angiograms. The seminal work by Prince was demonstrated on abdominal MRA, but soon thereafter CE-MRA techniques were refined for use in practically all anatomical regions (1–4). Due to its excellent image quality and speed, and spurred by improvements in MR hardware, software, and receiver coils, CE-MRA was rapidly adopted by the radiology, cardiology, and vascular communities for widespread routine clinical practice.

Development of modern NCE-MRA techniques has been motivated by several factors. Historically, Japan has been a source of NCE-MRA development due to the restriction of a maximum administration of 20 cc of contrast material per patient by the Japanese Ministry of Health, Labor, and Welfare (5). Perhaps the greatest source of Japanese interest in NCE-MRA stems from the persistently high cost of contrast material relative to clinical MR scan reimbursement by the Japanese medical establishment. Although contrast material is not as relatively expensive in other parts of the world, the added cost of contrast material combined with time, personnel, and equipment for set-up and administration of the contrast injection are additional motivators for the clinical use of NCE-MRA over CE-MRA.

Beyond cost-savings, safety-related motivations for avoiding contrast enhancement have compelled global development of NCE-MRA. Concerns about a possible link between gadolinium-based contrast agents and nephrogenic systemic fibrosis (NSF) have brought into question the use of these agents for MRA (6,7). While this link has not yet been conclusively proven, a correlative association has been identified by several studies (8–12). As a precaution, the U.S. Food and Drug Administration applied a black-box warning on gadolinium-based contrast agents in 2007 (13). Due to NSF concerns, it is recommended that special considerations be taken regarding the use of gadolinium-based contrast agents, especially for renal-compromised patients (7,14,15). The confounding factor is that it is often the renal-compromised patients who are the patient population that needs an MRA examination.

The recent renaissance in NCE-MRA owes as much to technical advancements in MR hardware and software as it does to its cost- and safety-related motivating factors. Multichannel receiver coil arrays generate higher signal-to-noise ratio (SNR), which can be exchanged for higher resolution. High bandwidth data acquisition hardware combined with faster and stronger gradients facilitate shorter TEs and TRs, enabling faster scan times, higher SNR, and/or higher-resolution images. The application of parallel imaging techniques in NCE-MRA has reduced shot durations and/or the total number of shots, thereby greatly reducing scan times (16,17). The higher field strength of the increasingly prevalent 3T scanners not only improves SNR, but also lengthens T1, resulting in reduced stationary tissue signal in inflow-based NCE-MRA and longer blood transit times for spin labeling NCE-MRA. Although these advancements have enabled the progress of MRI in general, since NCE-MRA methods have had traditionally longer scan times, lower resolution, and lower SNRs compared to CE-MRA, the combination of these technical improvements has been particularly important in making NCE-MRA applications feasible for routine clinical use.

This review article examines both established and recently developed NCE-MRA techniques. These techniques are categorized by their dominant mechanism: inflow, flow-dependency on cardiac phase, flow-encoding, spin labeling, and relaxation. The purpose of this review article is to explain the physical mechanism underlying each method and discuss their relative advantages and disadvantages. In particular, the characteristics of each technique are highlighted with regard to coverage efficiency, scan time, sensitivity to vessel orientation, vessel selectivity, venous contamination, and background suppression. For each technique a brief overview of the clinical applications is provided. A more detailed description of the clinical applications using these techniques can be found in complementary review articles (18–20). Other relevant principles of MRA, such as arterial and venous flow patterns and T1 and T2 values of arteries and veins, are discussed elsewhere (18–23).

Focusing on angiography, other general blood-flow-related techniques will not be explored including perfusion applications of spin labeling, quantification of cardiac function, or vessel imaging using black-blood methods. While noncontrast-enhanced venography can be accomplished with some of the techniques (24), the primary focus will be on arteriography.

INFLOW-BASED TECHNIQUES

General Mechanism of Inflow Effect

The oldest class of NCE-MRA techniques relies on the inflow effect of blood, also known as time-of-flight (TOF) (25,26). The inflow effect is the result of the difference in exposure to radiofrequency (RF) excitation of spins in stationary tissue versus spins in inflowing blood. Repeated RF excitation of a section (slice or slab) saturates stationary spins causing their longitudinal magnetization (M_z) to approach a low steady-state value ($M_z \approx 0$), resulting in low image signal intensity. However, inflowing blood entering the section arrives with fresh longitudinal magnetization ($M_z = 1$), resulting in high image signal intensity.

The inflow effect is dependent on the refilling rate of the section. The percentage of the blood that is refreshed within a section is a function of blood velocity, repetition time (TR), and cross-sectional area of the vessel (related to the section thickness). Figure 1 illustrates the inflow effect. For a simple plug-flow model, if blood velocity > thickness/TR, the entire volume of blood within the section is replaced between RF excitations. If the blood velocity is less than this critical replacement velocity, some portion of the blood volume will experience multiple RF excitations and become partially saturated. In this partial saturation regime the blood signal is dependent on the excitation flip angle and the T1 of blood. It is this flip angle/T1 dependency that CE-MRA exploits due to the fast gadolinium-assisted T1 relaxation of contrast-enhanced blood (1).

Inflow-based techniques are commonly paired with a flow-compensated readout to reduce signal loss from flow-induced spin dephasing (25,26). These flow-compensated gradient waveforms use extra gradient lobes to null gradient moments for both stationary spins and flowing spins moving through the gradient field. Flow-compensated gradient waveforms can be applied on either or all of the readout (RO), phase encode (PE), or slice select (SS) axes. Sequences like balanced steady-state free-precession gradient-echo (bSSFP, trueFISP, FIESTA, trueSSFP, bFFE) can also be used for MRA due to the inherent flow-compensation provided by the moment balancing of bSSFP.

General Limitations of Inflow-Based Techniques

In inflow-based techniques, any inflowing blood, whether from venous or arterial sources, arrives with fresh longitudinal magnetization ($M_z = 1$) and appears bright. Hence, the inflow-based techniques are prone to venous contamination. To generate an arteriogram with minimal venous contamination, venous suppression is often incorporated using a

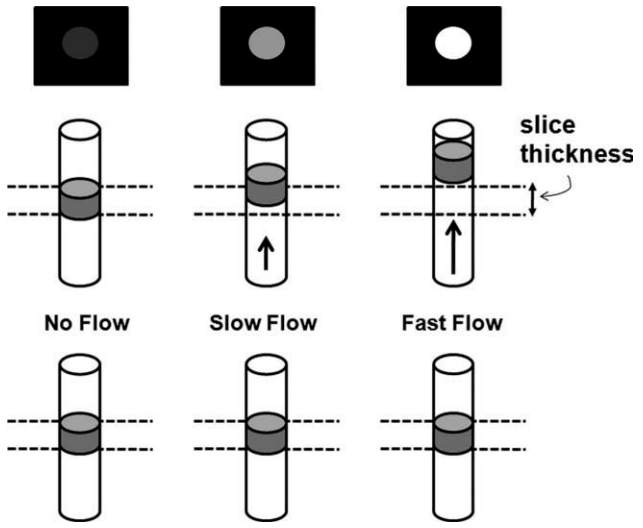

Figure 1. Illustration of the inflow effect. Bottom row: Spins within the imaging section (dotted lines) are excited by the excitation RF pulse. Middle row: After one TR period, stationary spins remain within the imaging section. Slow-flowing spins have partially flowed out of the imaging section and are partially replaced by fresh inflowing spins. Fast-flowing spins have flowed out of the imaging section and are completely refreshed by inflowing spins. Top row: pictorial images of the inflow effect. Stationary spins are repeatedly saturated and produce near zero signal. Slow-flowing spins are partially saturated and produce low signal. Fast-flowing spins are unsaturated at each excitation and produce high signal.

"walking" presaturation RF pulse. This selective presaturation RF pulse is applied to the venous upstream region relative to the imaging section. As the imaging section is spatially shifted to the next position, the venous presaturation region position is shifted proportionately to "walk" with the imaging section. In this way the relative distance between the venous presaturation region and the imaging section, and hence the venous suppression effect, is held constant.

The inflow effect is dependent on the vessel orientation relative to the imaging section. The optimal refreshment occurs for arteries running perpendicular to the thinnest dimension of the section volume. For vessels that lie generally in parallel with the imaging section their effective refreshment rate is very low. For this reason, inflow-based techniques are most applicable for vessels with preferential orientations like the carotid or peripheral arteries. For more tortuous vessels like renal arteries or distal peripheral arteries in the hand or foot, the refreshment rate is drastically reduced and hence inflow-based techniques are rarely used in these anatomies.

3D TOF

Description

The thick slab of 3D acquisitions poses a challenge for inflow-based techniques. The blood velocity needs to be very high to refresh the thick slab, so most often 3D TOF operates in the partial saturation regime. To address this issue the slab can be split into multiple,

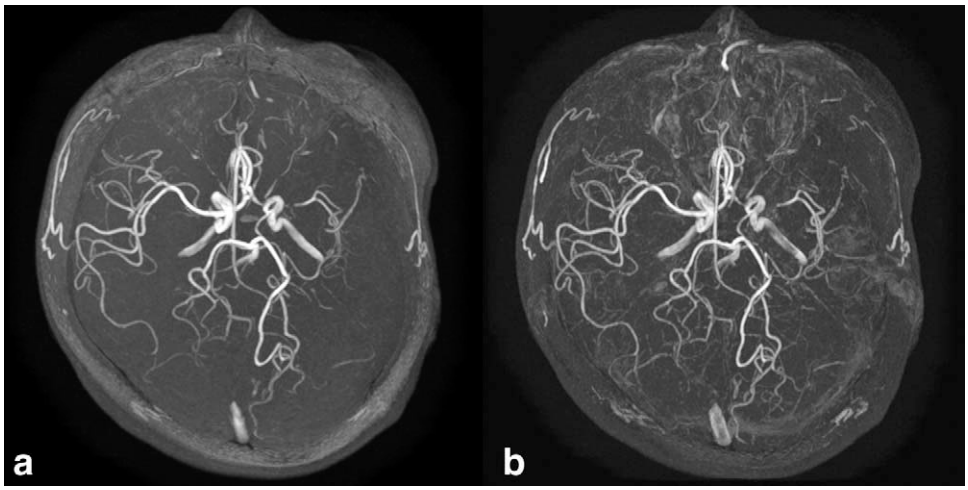

Figure 2. Comparison of axial projection MIP for (**a**) 3D TOF and (**b**) HOP-MRA at 3T on a 14-year-old girl with moyamoya disease. The HOP-MRA image shows increased conspicuity of small vessels compared to the conventional 3D TOF image. (Image courtesy of Dr. K. Tsuchiya, Kyorin University Hospital, Tokyo, Japan.)

thinner slabs. By using thinner slabs the critical replacement velocity is reduced, resulting in increased inflow refreshment. Often, the multiple slab coverages are partially overlapped, reducing coverage efficiency. Further enhancements to the thin slab approach include multiple overlapping thin-slab acquisition (MOTSA) (27,28). This hybrid 2D/3D method is designed to greatly reduce the effective selection thickness and increase the inflow effect. To further reduce blood saturation, the slab can be excited using an RF excitation pulse with ramped slice selection profile like the tilted optimized nonsaturating excitation (TONE) pulse (29). The TONE pulse reduces saturation for spins entering the slab by using a low flip angle at the inflow edge and a higher flip angle at the outflow edge. To further suppress stationary tissue signal, a nonselective off-resonance magnetization transfer (MT) RF pulse can be applied to reduce the signal of brain parenchyma (29–31). Brain parenchyma is more susceptible to MT saturation than blood due to its greater relative macromolecular content.

Applications

The most common application of 3D TOF is intracranial angiography (25–36). In particular, 3D TOF has been used for diagnostic imaging of intracranial occlusions (32,33) as well as aneurysms (34,35). The high resolution of the 3D acquisition provides excellent depiction of small intracranial vessels. Since physiological motion is negligible in the head, long scan times (>5 minutes) to acquire high-resolution images are acceptable (36).

HOP-MRA

Description

The hybrid of opposite-contrast (HOP) MRA method is an extension of 3D TOF (37). The HOP-MRA pulse sequence begins with a flow-compensated echo acquisition, similar to conventional 3D TOF. The first echo is typically flow-compensated in all three axes. Within the same TR, following the first flow-compensated echo, a second flow-spoiled echo is acquired. Between the first and second echoes, flow-dephasing bipolar gradients (see Flow-Encoding section for further description) are applied to all three axes to dephase flowing spins, which results in a dark appearance of blood. The echo data are reconstructed into two separate images: bright-blood and dark-blood. Since it is fundamentally 3D TOF, the bright-blood image depicts fast-flowing blood better than slow-flowing blood. On the other hand, the dark-blood image generates negative contrast even for slow-flowing spins, including those in small branch arteries. The bright-blood and dark-blood images are combined using subtraction to yield a final angiogram (38). The combined angiogram benefits from the strengths of each source image; it is able to depict vessels with both fast- and slow-flowing blood in a single angiogram created from a single scan. Furthermore, stationary tissue signal is mostly eliminated via subtraction, thereby enhancing vessel depiction.

Applications

The intended application of HOP-MRA is the same as 3D TOF: intracranial angiography (37–39). Figure 2 illustrates the additional fine vessel structure depicted by HOP-MRA compared to conventional 3D TOF.

2D TOF

Description

The thinner sections of 2D TOF allow faster inflow refreshment and increased arterial signal compared to 3D TOF-based methods. However, since the 2D slice thickness is typically larger (≥3 mm) than the slice resolution of 3D TOF (≤1 mm), the 2D TOF approach is commonly used only for angiography of large gauge vessels. Often, the 2D slices are acquired with some overlap to reduce the discontinuities at the slice edges in a maximum intensity projection (MIP) depiction of the data—often called the "stairstep artifact" (40,41). This 2D overlap reduces the coverage efficiency of the technique. The 2D TOF technique is notorious for depicting false stenoses at the carotid notch due to reduced inflow refreshment caused by the angle of the vessel orientation (42). Also, the 2D TOF technique commonly generates signal voids in the carotid bulb due to recirculating flow patterns (43).

Figure 3. Coronal MIP of a multi-station peripheral run-off study on a volunteer using QISS. Axial QISS data were acquired with 1 × 1 mm in-plane resolution and 3 mm effective slice thickness (interpolated to 1.5 mm). In this example, the total scan time for all stations was approximately 6 minutes 30 seconds. (Image courtesy of Dr. R. Edelman, NorthShore University Health System, Evanston, IL.)

Applications

The 2D TOF technique is commonly used for imaging vessels with preferentially perpendicular flow and relatively fast velocity like peripheral (41) and carotid (43) arteries. It has been demonstrated for the evaluation of stenosis in tibial and pedal arteries (41). In peripheral applications, 2D TOF is often combined with systolic gating to capture the period of greatest blood velocity, and hence greatest inflow effect.

QISS

Description

Recently, an inflow-based NCE-MRA technique called quiescent interval single-shot (QISS) has been developed (44). The QISS technique relies on a presaturation RF pulse to saturate the signal in the imaging slice. Following the presaturation, during a "quiescent interval" (QI) fresh inflowing blood enters the saturated slice. The signal is quickly acquired using a single-shot 2D bSSFP sequence. The trigger delay is adjusted so systole occurs during the QI and signal acquisition occurs during diastole. By aligning the QI with systole, maximum inflow is achieved. The 2D slice is moved sequentially from foot to head so the slice can be continually filled with fresh, unsaturated, inflowing blood. The QI is designed to be long enough to allow adequate inflow, but short enough to maintain saturation of the stationary tissue signal. Since the QI is relatively long compared to the short T1 of fat, a fat saturation prepulse is commonly applied immediately prior to bSSFP readout.

QISS differs from 2D TOF with regard to sensitivity and speed. The inflow refreshment effect is much greater for QISS than 2D TOF. The QI period (≈230 msec) allows for a relatively long time for inflow refreshment compared to a typical TR of 2D TOF (≈30 msec). This greatly reduces the critical replacement velocity, thus making QISS able to depict slow-flowing blood. For a 3-mm slice, full inflow refreshment can be achieved for QISS by blood flowing at 1.3 cm/s versus 10 cm/s for the equivalent 2D TOF slice.

Applications

The use of QISS is dictated by some of the same limitations as 2D TOF. The slice orientation of QISS should be perpendicular to the general vessel orientation to improve the inflow effect. Therefore, its most common application is for run-off studies in peripheral arteries (Fig. 3) (44). Due to its use of the bSSFP readout, QISS requires good B_0 homogeneity across the image volume. Therefore, the useable extent of field-of-view (FOV) and slice coverage is limited by the quality of the static magnetic field (B_0) shim. Accordingly, QISS is often performed with a greater number of smaller coverages with reshimming between each coverage acquisition. Since QISS acquires a complete slice in one cardiac R-R period (≈1 sec), QISS is able to cover a 15-cm region using a 3-mm slice thickness in 1 minute versus 5 minutes for 2D TOF with similar parameters. A multi-station run-off study (iliac to calf station) using QISS takes ≈8–10 minutes, not including time for repositioning or reshimming.

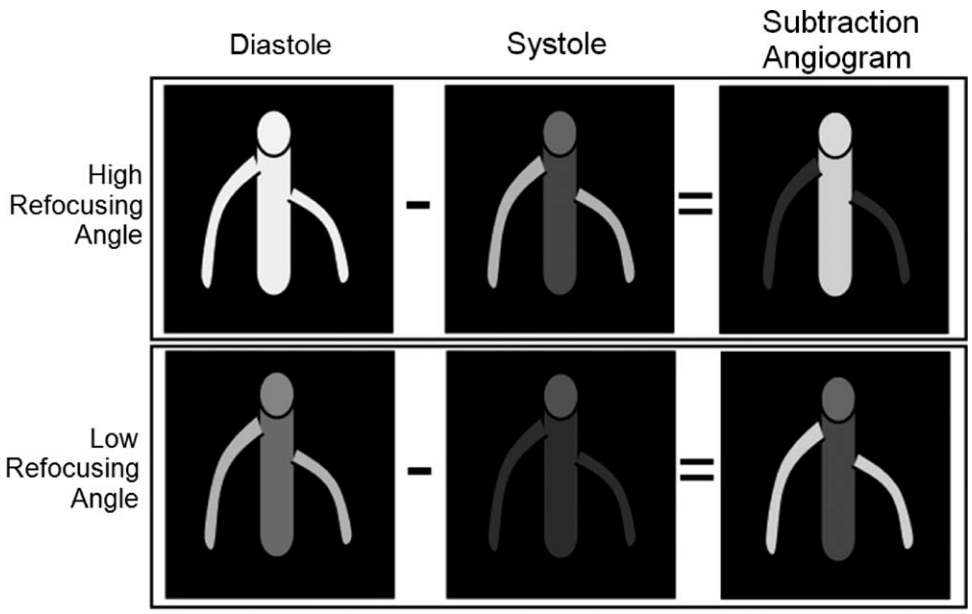

Figure 4. Illustration of the effect of refocusing flip angle on vessel signal in diastole (bright-artery scan) and systole (dark-artery scan). The large central artery contains fast-flowing blood and the two smaller branch arteries contain slow-flowing blood. With high refocusing angles, although the small vessels are relatively bright in both systole and diastole scans, due to subtraction, they appear dark in the angiogram. Due to low refocusing angles, the large artery signal is reduced in both diastole and systole scans, resulting in weak depiction in the subtraction angiogram.

CARDIAC PHASE-DEPENDENT TECHNIQUES

General Mechanism of Flow-Dependency on Cardiac Phase

The cardiac-phase-dependent class of NCE-MRA techniques relies on the physiologic difference in arterial flow velocity between systolic and diastolic cardiac phases. During systole, arterial flow is fast, whereas during diastole arterial flow is slower. In contrast, venous flow is nonpulsatile and relatively slow (<5 cm/s) throughout the cardiac cycle.

This general class of NCE-MRA techniques leverages the motion sensitivity of pulse sequences to produce dark-artery (DA) image sets acquired during systole and bright-artery (BA) image sets acquired during diastole. The DA image set is subtracted from the BA image set to create the angiogram. Ideally, the signal from stationary tissue in both image sets is identical and therefore cancels in the final subtracted image. The motion-sensitization of the technique can be generated or accentuated in several ways, which is further described below.

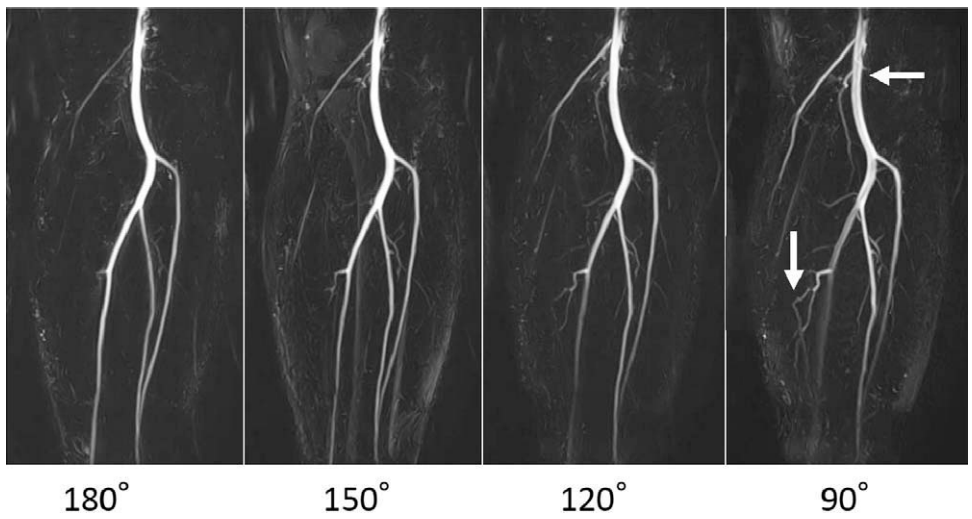

Figure 5. Example of the cardiac-gated 3D FSE NCE-MRA method in the popliteal region. Each image is a coronal MIP of the coronally acquired 3D FSE image volume. The corresponding refocusing angle used in the FSE acquisition is listed below each MIP. The horizontal arrow near the femoral artery highlights the signal loss in large arteries due to the low refocusing angle. The vertical arrow near the posterior tibial artery highlights the improved depiction of branch vessels with low refocusing angle.

Cardiac-Gated 3D Fast-Spin-Echo NCE-MRA

Description

The fast-spin-echo (FSE, or turbo-spin-echo TSE) sequence, including half-Fourier FSE or single-shot FSE, is inherently sensitive to motion. Spins flowing out of the imaging section during the echo train cannot be repeatedly refocused by the RF refocusing pulses. This signal void is the premise behind thin-slice black-blood 2D FSE (45). However, in NCE-MRA, thick-slab 3D FSE is used, so this source of flow-related signal loss is minor and little flow-spoiling is observed in the slice direction. The strongest flow-spoiling effect for 3D FSE is in the RO direction due to the alternate echo flow-spoiling effect caused by the RO gradients in the echo train. In both the slice and RO directions, the flow-spoiling effect is exacerbated by the use of sub-180° refocusing flip angles in the echo train, resulting in even greater signal loss. Essential concepts related to angiography applications of FSE, including flow-compensation (46), gradient moment nulling (47), and the T2-blurring effect (48,49) are discussed elsewhere.

The inherent flow-spoiling of FSE is the underpinning of cardiac-gated 3D FSE NCE-MRA. The original 2D projection spin-echo-based technique (50,51) was later refined and extended to a 3D NCE-MRA technique (52,53). Cardiac-gated 3D FSE NCE-MRA produces images with dark signal (flow void) in arteries with fast-flowing blood to create the systolic DA scan. The slower blood flow during diastole generates high arterial signal in the BA scan. Since the venous flow is relatively constant in both image sets, venous contamination is effectively removed via subtraction in the final angiogram. This method is available commercially as FBI, NATIVE SPACE, 3D Delta Flow, and TRANCE.

The fast-spin-echo readout commonly uses only one or two shots per slice encoding value to minimize total scan time. Each shot uses a partial-Fourier echo train to shorten the echo train length to reduce T2-blurring. The RO direction is typically selected to be in parallel with the general direction of flow to accentuate the flow-spoiling effects of FSE (54). The scan is triggered with either electrocardiographic (ECG) or peripheral pulse gating (PPG). The ideal systolic and diastolic trigger delay times are calibrated per patient. Often, the image sets are acquired with fat suppression, typically using short-tau inversion recovery (STIR) or spectrally adiabatic inversion recovery (SPAIR). While fat suppression is not strictly necessary due to the subtraction step which removes stationary tissue signal, the removal of fat improves the image quality in the native DA and BA source image sets since they are often diagnostically evaluated alongside the subtracted angiogram (54). The DA and BA image sets are acquired in direct succession to mitigate patient motion and reduce image misregistration. Thus, the total scan time for both systolic and diastolic acquisitions using cardiac-gated 3D FSE NCE-MRA is in the range of 3–4 minutes (54). A typical multi-station run-off study (iliac to calf station) takes ≈10–12 minutes, not including time for repositioning or recalibration of cardiac delay times (54).

The motion sensitivity of cardiac-gated 3D FSE NCE-MRA techniques is influenced by the choice of refocusing flip angle (55). The refocusing flip angle affects the relative depiction of fast-flowing blood in large arteries versus slow-flowing blood in smaller branch arteries, as illustrated in Figure 4 and exemplified in Figure 5. High refocusing flip angles (160°+) produce very bright signal in BA scans, but also refocus more signal in arteries with slow-flowing blood in DA scans. Thus, a high refocusing flip angle produces a subtraction angiogram with bright signal for large arteries, but weak signal for small arteries. Low refocusing flip angles (<120°) produce lower signal for large arteries in BA scans, but small arteries with slower diastolic flow are less affected. The low refocusing angle accentuates the FSE flow-spoiling effect, resulting in reduced arterial signal in the DA scan, even in smaller arteries with slow-flowing blood. Thus, a low refocusing flip angle produces a subtraction angiogram with greater signal intensity in smaller arteries and less signal intensity in larger arteries. Accordingly, the proper refocusing flip angle can be tuned depending on the arteries of interest.

In a similar fashion, the flow sensitivity of cardiac-gated 3D FSE NCE-MRA can also be adjusted by adding additional flow-dephasing or partially flow-compensating gradient lobes in the RF echo train (53,54). If additional flow-dephasing is added, the scan is able to better depict slow-flowing blood. In the same manner as the lower refocusing flip angle, using readout gradients with additional flow-dephasing generates a subtraction angiogram with relatively higher signal in smaller arteries and weaker signal in larger arteries. To better depict fast-flowing blood in large arteries, such as the iliac, partially flow-compensating readout gradients are commonly applied for the opposite effect. The partial flow-compensation makes the readout gradients become less susceptible to signal loss caused by flow-induced dephasing. Thus, similar to the use of a high refocusing angle, the BA scan and the DA scan both produce high signal for slow-flowing blood in small arteries. The result is a subtraction angiogram with bright signal in large arteries and weaker signal in smaller arteries.

Unlike the inflow-based techniques, the choices of FOV and section thickness have no impact on the angiographic applications of the technique, other than simple SNR and coverage efficiency considerations. Since the cardiac-gated 3D FSE NCE-MRA readout method is insensitive to B_0 inhomogeneity, cardiac-gated 3D FSE NCE-MRA can be used with robust results near susceptibility fields (lungs) or with large FOV coverage.

The cardiac-gated 3D FSE NCE-MRA techniques have some fundamental limitations. Since these techniques are cardiac-gated, they are sensitive to the effects of arrhythmia or trigger delay calibration errors. Due to the requirement of two scan acquisitions and multiple R-wave intervals, the methods are generally slow. Due to the inherent flow-spoiling effects of FSE, very fast and/or turbulent flow, like poststenotic flow, generates a flow void even in the BA scan (42). Since the BA scan and the DA scan depict

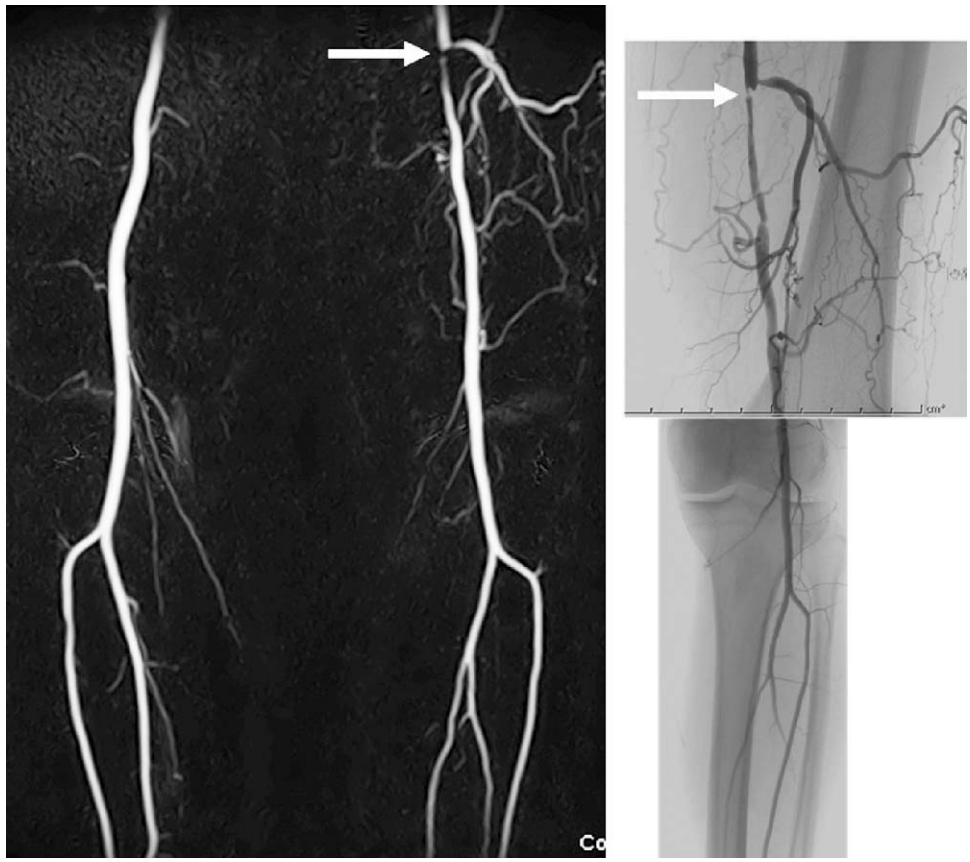

Figure 6. Example of cardiac-gated 3D FSE NCE-MRA (left) compared to x-ray digital subtraction angiography (right) on a patient with peripheral occlusive disease. The occlusion is indicated by an arrow on each image. (Image courtesy of Dr. J. Levine, Little Company of Mary Hospital, Evergreen Park, IL.)

vessels with low signals in this region, a signal void appears in the subtraction angiogram leading to a tendency toward overestimation of stenosis. This overestimation can be mitigated by evaluation of BA images in conjunction with the subtraction angiogram (54).

Applications

The large coronal FOV coverage, robustness to B_0 inhomogeneity, inherent venous suppression, and insensitivity to vessel orientation enable the widespread application of cardiac-gated 3D FSE NCE-MRA. Since the FSE readout can capture vessel signal close to air–tissue interfaces, a common application is pulmonary angiography. Cardiac-gated 3D FSE NCE-MRA has been used in angiography of the thoracic and abdominal aorta (5). Near the thoracic and abdominal aorta, the acquisition can be performed with a single diastolic BA scan to produce an angiogram with minimal background signal since venous and stationary tissues are largely absent in this region.

The cardiac-gated 3D FSE NCE-MRA method is well suited for peripheral run-off MRA due to its large volume coverage. Several clinical studies comparing cardiac-gated 3D FSE NCE-MRA to computed tomography angiography (CTA) (54) and CE-MRA (56,57) in peripheral run-offs reported high diagnostic scores of sensitivity (97%, 85.4%, and 100%, respectively) and negative predictive value (NPV) (99%, 92.3%, and 100%, respectively). However, the clinical studies reported lower diagnostic scores for specificity (96%, 75.8%, and 72.7%–85.5%, respectively) and positive predictive value (PPV) (88%, 74.1%, and 66.7%–78.2%, respectively). In addition, the CE-MRA comparison studies (56,57) reported that 47.2% and 42.4%, respectively, of segments in cardiac-gated 3D FSE NCE-MRA data were deemed nondiagnostic due to image artifacts.

A modified cardiac-gated 3D FSE NCE-MRA technique using variable flip angles has also been applied in angiography of the hands at 3T incorporating additional flow-dephasing gradients to enhance the depiction of slow-flowing blood in the arteries of the extremities (58). Figure 6 shows an example of cardiac-gated 3D FSE NCE-MRA and x-ray digital subtraction angiography (DSA) on a patient with peripheral occlusive disease.

FLOW-ENCODING TECHNIQUES

General Mechanism of Flow-Encoding

In the same way that magnetic field gradients can be used to encode the spatial position of spins, they can be used to encode the motion, or flow, of spins. Spins in the transverse plane flowing in the vector direction of a gradient field accumulate phase proportional to their speed. In this way, the flow velocity (direction and speed) is encoded in the phase of the spins. Bipolar gradients consisting of two equal but opposite amplitude gradient lobes are commonly used for flow-encoding. The bipolar gradients generate net zero phase for stationary spins but a nonzero phase for flowing spins related to the amplitude and duration of

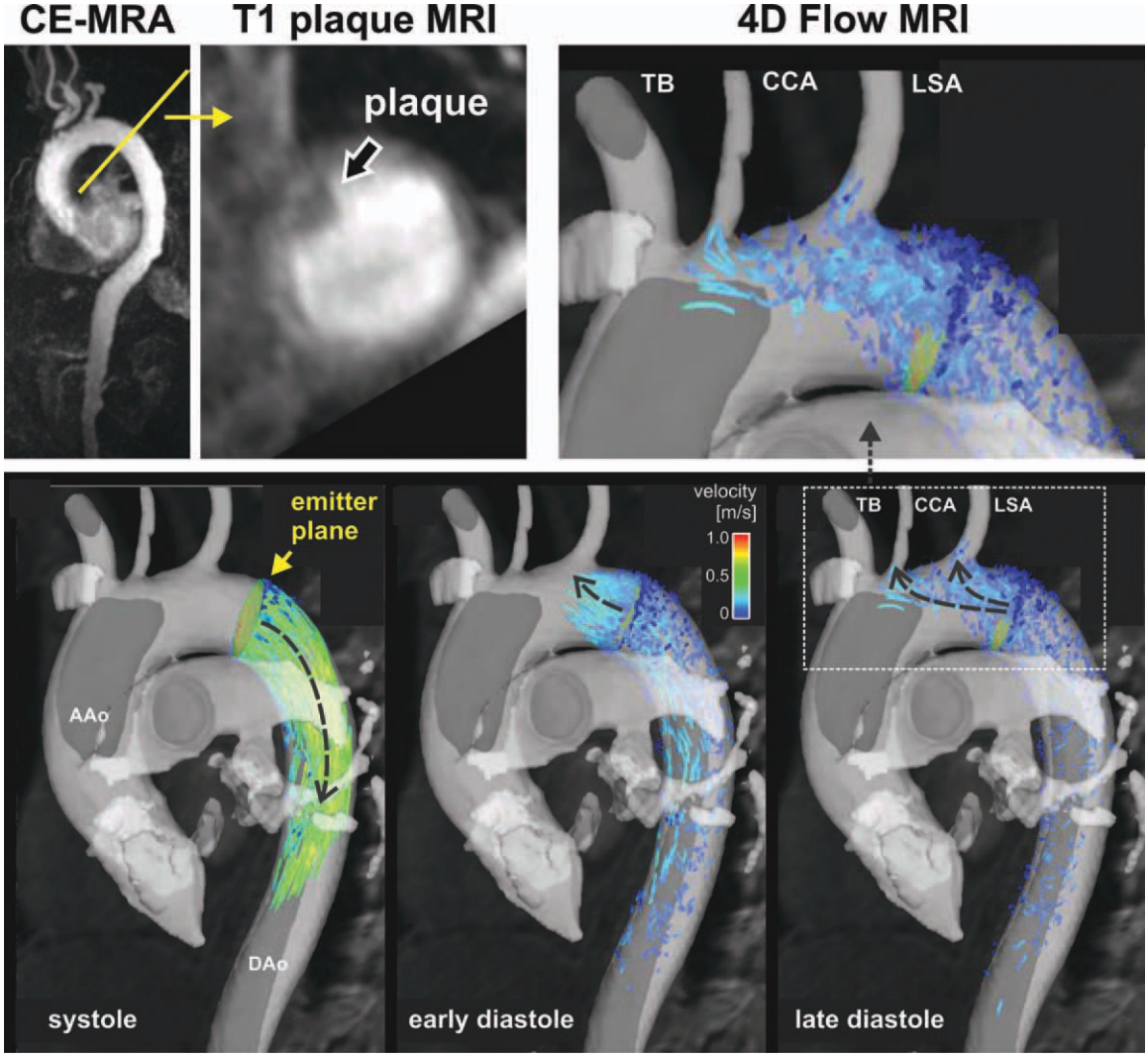

Figure 7. Top row: CE-MRA and 3D T1 plaque MRI used for detecting the location and size of aortic high-risk plaques. The plaque image shows a hypointense structure protruding into the proximal descending aorta (DAo) with a superimposed mobile thrombus ≥8 mm. CE-MRA indicates plaque localization. Lower row: An emitter plane positioned at the location of the aortic plaque was used to generate time-resolved 3D particle traces, which resemble the temporal and spatial evolution of blood flow throughout the cardiac cycle. The series of images show systolic forward flow followed by substantial diastolic retrograde flow. Marked diastolic retrograde flow originating from the location of the plaque in the proximal descending aorta is clearly evident and reaches two of three brain-feeding arteries. This mechanism thus indicates a risk for retrograde embolization in the brain stem and left hemisphere in the case of plaque rupture. (Image courtesy of Dr. M. Markl, Northwestern University, Chicago, IL.)

the bipolar gradient lobes. Alternatively, the flow-induced phase can be used for simple flow-dephasing instead of flow-encoding.

Conventional Phase Contrast

Description

Phase contrast MRA (PC-MRA) uses flow-encoding bipolar gradients to generate quantitative flow images (59–61). Since the flow information is encoded in phase, for PC-MRA, phase rather than magnitude images are reconstructed. For the simplest case of 1D flow quantification, two PC scans are acquired. Typically, alternate bipolar polarities are used (+/− followed by −/+). By subtracting the two flow-encoded PC phase images, the background phase accrual is removed. Since stationary spins have zero net phase after the subtraction, stationary tissue signals are inherently suppressed in the displayed phase difference images. Quantitative measurements of flow velocity can be calculated from the phase data using the explicit relationship between velocity and bipolar gradient amplitude and duration. These quantitative data are presented as a flow map.

Since the bipolar gradients can be applied in any combination of RO, PE, or SS axes, PC-MRA can be used to measure directionality of flow as well as speed. Thus, PC-MRA has the advantage of depicting multidirectional flow, including recirculating flow patterns. Unlike inflow-based techniques, which require blood to flow through the slice to be visible, PC-MRA

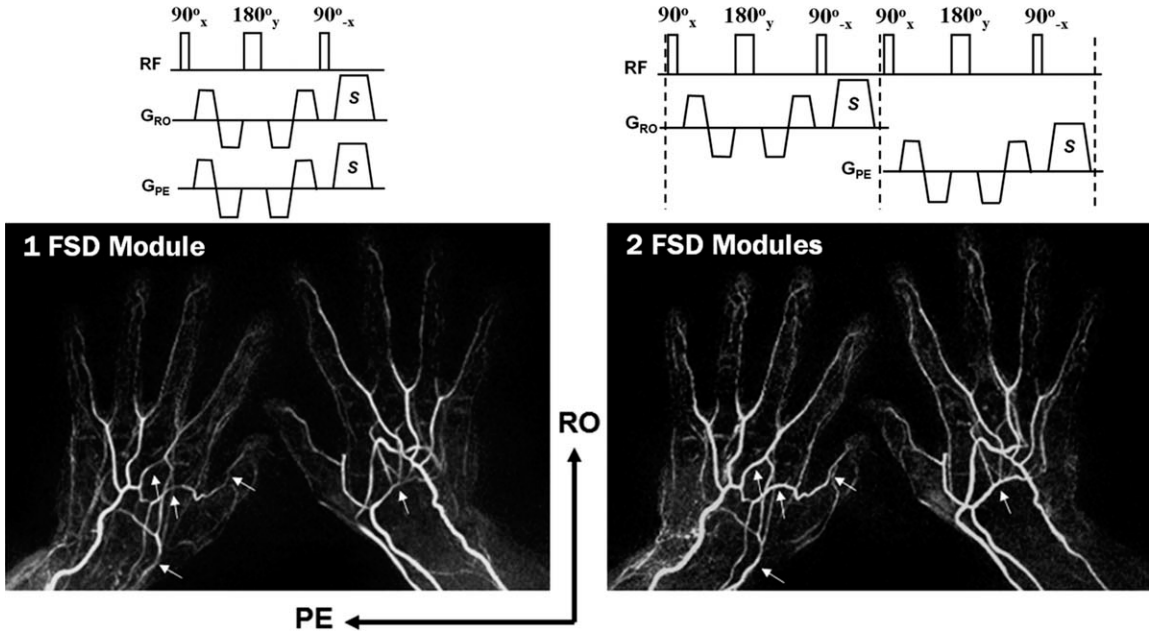

Figure 8. Example of FSD in the digital arteries. By using two FSD modules in succession with orthogonal flow-dephasing gradient directions (RO axis followed by PE axis), the arterial depiction is improved compared to using only one FSD module with a single flow-dephasing gradient direction (simultaneously applied on RO and PE axes). The arrows on the images indicate vessels with signal improvement using the two-module versus the one-module approach. (Image courtesy of Dr. Z. Fan, Northwestern University, Chicago, IL.)

can detect flowing blood that remains within the slice. In its simplest form, PC-MRA requires two images to generate flow data in a single direction. To visualize flow in orthogonal directions, additional directional pairs must be acquired at the cost of adding proportionally more scan time.

Applications

Due primarily to its long scan times, PC-MRA is not commonly used for routine MRA beyond specific niche applications. Its most common angiographic use is as a low-resolution scout sequence for identifying the location of the carotid arteries. PC-MRA has also been used to distinguish the degree of stenosis in renal (62) and carotid (63) arteries.

4D Flow

Description

An emerging application of PC-MRA is the measurement of flow dynamics with 4D flow mapping (64). The fourth dimension in this application is time. The technique generates time-resolved 3D PC flow maps acquired with cine mode ECG gating. The fundamental techniques behind 4D flow have existed for some time, but only recently have hardware and software advances enabled the time resolution of the acquisition as well as the processing and visualization capabilities to generate high-quality results.

Applications

Visualization of hemodynamics using the 4D flow technique affords a comprehensive evaluation of regional aortic flow characteristics. The 4D flow technique has been applied to the measurement of aortic pulse wave velocity (65) and wall shear stress (66) for the purposes of identifying potential emboli from high-risk atherosclerotic plaque (67). Figure 7 shows an example of 4D flow analysis of atherosclerotic plaque in the aorta.

Flow-Sensitive Dephasing

Description

Recently, an alternative flow-encoding-based technique called flow-sensitive dephasing (FSD) has been developed (68). The FSD module consists of a 90°(x)-180°(y)-90°(−x) spin-echo interspersed with optional flow-encoding bipolar gradients (Fig. 8). In the FSD technique, the flow-induced phase generated by the bipolar gradients is not used for flow-encoding, but rather flow-dephasing. At the RF echo, the flipback 90°(−x) RF pulse restores rephased transverse magnetization in stationary tissue to the longitudinal axis. The dephased spins in flowing blood remain in the transverse plane to be further crushed by the trailing gradient. The motion sensitivity of FSD can be controlled by the amplitude and duration of the bipolar gradient lobes. This sensitivity is commonly referred to in the literature as "m1" in reference to the first-order moment the flow-dephasing gradients impart on flowing spins. High m1 corresponds to strong flow-dephasing effect, whereas m1 = 0 corresponds to no flow-dephasing.

The FSD technique also relies on the general mechanism of flow-dependency on cardiac phase. The DA scan is acquired with high m1 during systole using ECG or PPG gating. Specifically, the trigger delay is calibrated to align the timing of the FSD prepulse

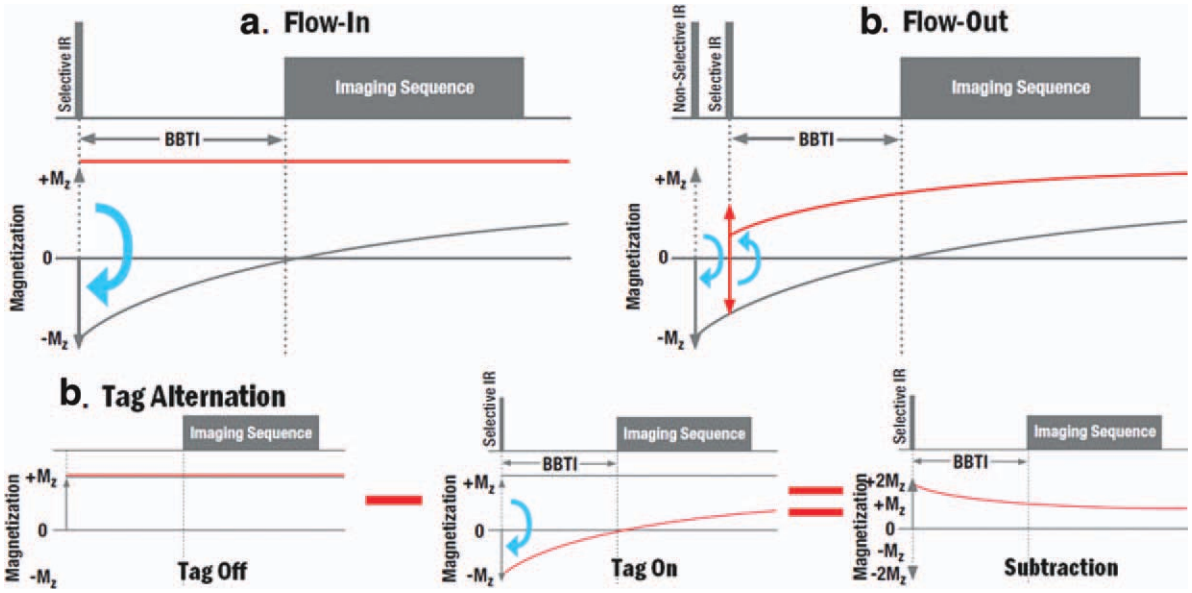

Figure 9. Illustration of the different spin labeling methods: (**a**) flow-in, (**b**) flow-out, and (**c**) tag-alternation. Refer to Figure 10 for an illustration of the tag placement relative to the image volume for each method. A: Flow-in: following a selective inversion pulse (typically corresponding to spatial region of the imaging volume) blood (red line) with fresh magnetization flows into the imaging volume during the BBTI period while the stationary tissue (gray line) undergoes T1 recovery. Data acquisition occurs near the null point of stationary tissue. B: Flow-out: An initial nonselective inversion pulse inverts all magnetization. Immediately afterward, a selective inversion pulse, applied to a separate vessel tagging region, restores magnetization only within the tagging region. During the BBTI, the restored blood flows into the imaging volume while stationary tissue undergoes T1 recovery. C: Tag-alternation: the tag-off acquisition acquires an image with blood and stationary tissue with positive magnetization. The tag-on acquisition uses a selective inversion pulse (applied to a separate vessel tagging region) to invert magnetization only within the tagging region. During the BBTI, the inverted blood flows into the imaging volume. The subtraction of tag-on from tag-off data produces an angiogram with positive signal in regions fed by inflowing blood and null signal in stationary tissue.

with the arrival of the systole bolus. The high m1 of the flow-dephasing gradients generates low arterial signal in the DA scan. The BA scan is acquired with m1 = 0 during diastole, resulting in high arterial signal. The DA magnitude image set is subtracted from the BA magnitude image set to create the final angiogram. Like any subtraction-based technique, the requirement of two scans increases scan time. Typical total scan times are similar to cardiac-gated 3D FSE NCE-MRA at 3 to 4 minutes. The FSD module is typically appended to a flow-compensated sequence like bSSFP so the total flow-spoiling effect is dominated by the choice of m1 and not the readout sequence itself. Like cardiac-gated 3D FSE NCE-MRA, FSD commonly uses a 3D acquisition to acquire good slice resolution by acquiring in a coronal orientation.

Since all flowing spins produce a signal difference in the BA-DA subtraction of FSD, venous signal can also appear in the final subtracted angiogram. The amount of venous contamination can be controlled by selecting an optimal value of m1 (69). High m1 generates a strong signal difference between BA and DA scans, thus generating bright arterial signal in the angiogram. However, a high m1 also produces a large signal difference between BA and DA scans in veins, resulting in venous contamination. A low m1 only weakly dephases the slowly flowing venous spins in the DA scan, resulting in little venous contamination in the angiogram. But a low m1 reduces the signal difference between BA and DA scans for arteries, particularly slow-flowing arteries, resulting in a loss of arterial signal in the angiogram. Therefore, m1 needs to be calibrated based on a trade-off between arterial signal loss and venous contamination (69).

The primary advantage of FSD is the high vessel signal in the BA scan. Since the bSSFP readout method is flow-compensated, all vessels are well-depicted in the BA scan, regardless of velocity. In comparison, the inherent flow-spoiling effect of the FSE readout in cardiac-gated 3D FSE NCE-MRA causes some arterial signal to be lost even in the BA scan, especially in vessels with fast-flowing blood. Compared to the FSE readout of cardiac-gated 3D FSE NCE-MRA, the bSSFP readout of FSD provides high SNR and sharp image resolution due to the lack of T2-blurring. This feature enables FSD to produce high-resolution angiograms particularly useful for depicting small vessels in feet and hands. The use of bSSFP requires good B_0 homogeneity. Thus, similar to QISS, the extent of applications is determined by the quality of static magnetic field (B_0) homogeneity. Therefore, the FSD technique may potentially struggle with large volume coverage or near areas with strong susceptibility fields (eg, lungs).

The flow-dephasing effect is related to the direction of blood flow relative to the direction of the flow-dephasing gradients. Thus, blood flow perpendicular to the flow-dephasing direction is not affected at all and does not appear in the FSD-generated angiogram. To address this orientation-sensitivity issue, at the

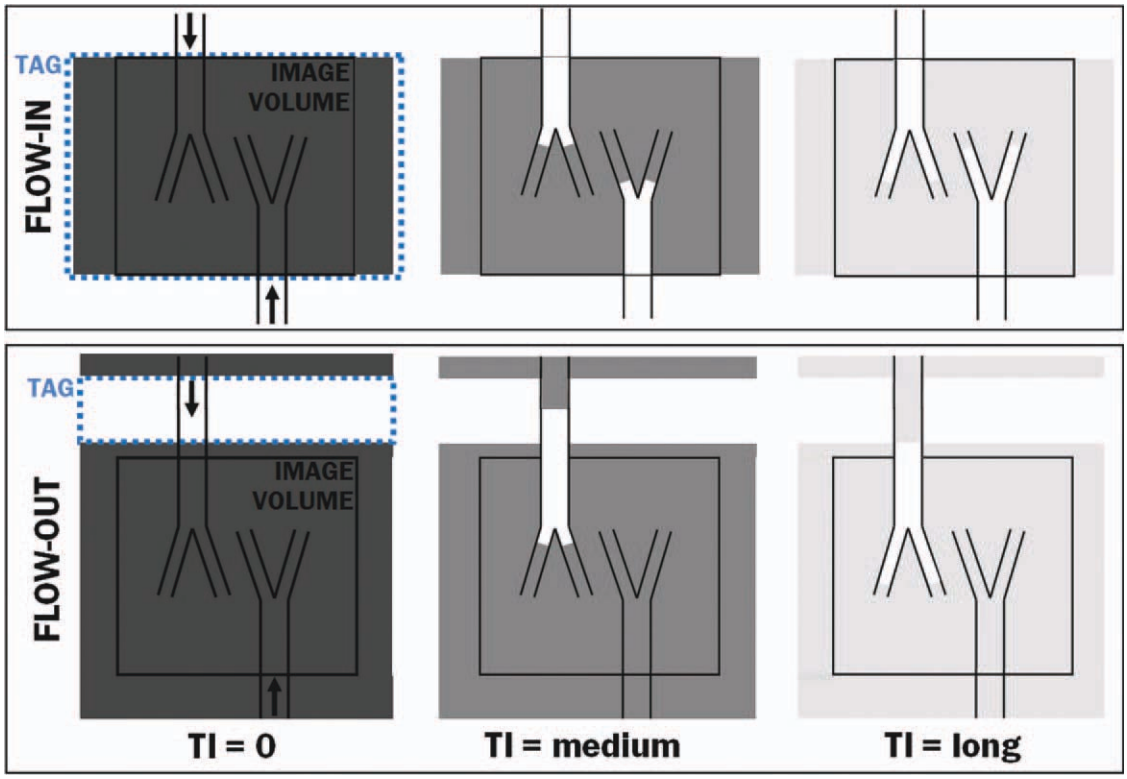

Figure 10. Illustration of flow-in and flow-out spin-labeling. The blue dotted box represents the selective tag region. The image volume (black box) is fed by two arteries. The direction of flow for each artery is indicated by arrows. The grayscale color represents longitudinal magnetization with white corresponding to positive ($M_z = 1$) and dark gray corresponding to negative ($M_z = -1$). Top row: Flow-in spin labeling. The tag region typically corresponds to the imaging volume, although they need not be identical. At TI = 0, all spins within the tag region are inverted. After medium TI, fresh magnetization from outside the tag has flowed into the vessels. At long TI, the blood has flowed into the distal branches. Stationary tissue signal has recovered by T1 relaxation, reducing contrast. Bottom row: Flow-out spin labeling. In this illustration, the tag region was drawn above the imaging volume. However, the tag region can be selected, rotated, and positioned independent of the imaging volume. At TI = 0, only the tagged region contains positive longitudinal magnetization; all other magnetization is inverted. At medium TI, blood has flowed out of the tag region and into the imaging volume. Only the vessel fed with tagged blood is depicted in the image. At long TI, blood has flowed into the distal branches of the tagged vessel while stationary tissue signal has recovered.

cost of SNR loss due to T2 decay, additional FSD modules with orthogonal flow-dephasing directions can be included. For example, FSD modules with bipolar gradients on the RO axis and PE axis can be applied sequentially to dephase all in-plane blood flow (70).

Applications

The FSD technique has been applied to peripheral arteries using a single module with flow-dephasing in the craniocaudal direction (68,69,71). The total acquisition time for a 40-cm coverage is 3–4 minutes, similar to cardiac-gated 3D FSE NCE-MRA. Using the two-module approach, depiction of the tortuous vessels in the hand can be achieved (70). Figure 8 shows the application of the two-module approach to depict the small vasculature of the digital arteries in exquisite detail.

SPIN LABELING TECHNIQUES

General Mechanism of Spin Labeling

The general technique of arterial spin labeling (ASL) uses some form of a selective inversion pulse to label or "tag" the longitudinal magnetization of inflowing blood. This tag can be applied in many ways, but the fundamental purpose is to force the longitudinal magnetization of flowing blood to differ from that of stationary tissue. Following the tagging, an inversion recovery delay period (TI) allows blood to flow into the imaging slab, after which it is read out with a conventional sequence. Spin labeling can be applied using three methods: flow-in, flow-out, and tag-alternation. The names "flow-in" and "flow-out" are in reference to the flow direction relative to the selective tag. Figure 9 illustrates the basic pulse sequence for each method. A pictogram of the typical flow-in and flow-out tag placements is provided in Figure 10.

Flow-In Spin Labeling Method

Description

In the flow-in method, the tagging pulse is applied to the entire imaging slab (Fig. 10). The tag inverts both blood and stationary spins in the region of interest. During the TI, fresh inflowing blood enters the imaging slab while the spins in stationary tissue and blood preexisting in the imaging volume return toward null

Figure 11. Example of renal NCE-MRA using flow-in spin labeling. Coronal MIP image of a 37-year-old healthy volunteer. The image was acquired using the flow-in technique with a spatially selective IR pulse applied to a volume containing the kidneys. A presaturation pulse was applied inferior to the renal region to achieve venous suppression.

magnetization ($M_z \approx 0$) via T1 recovery (Fig. 9a). The imaging slab is then read out using any conventional sequence. The fresh inflowing blood is depicted with bright signal due to its full amplitude longitudinal magnetization. If the TI approximately matches the null point of stationary tissue, the background signal is dark. These techniques are available under the commercial trade names of time-SLIP, NATIVE true-FISP, Inflow-IR, and b-TRANCE.

Applications

The most common clinical application of flow-in spin labeling NCE-MRA is renal angiography. The complex orientations of the aorta and renal arteries dictate the use of bSSFP due to its inherent multidirectional flow-compensation. The flow-in method is commonly used with a tag over the kidneys (Fig. 11). Flow-in spin labeling in conjunction with a respiratory real-time motion correction technique has been used to depict the renal arteries (72). Renal flow-in spin labeling NCE-MRA has been compared to CTA (73) and DSA (74,75) in several clinical studies. Similar to other NCE-MRA techniques, the clinical comparison studies (73–75) report high sensitivity (100%, 100%, and 93%, respectively) but lower specificity (93%, 88%, and 88%, respectively) for flow-in spin labeling versus

Figure 12. Example of the flow-out spin labeling method used for time-resolved NCE-MRA of the left carotid artery. Shown are MIP projections for TI from 400 msec to 1200 msec. Note that as the TI increases, stationary tissue signal starts to recover. (Image courtesy of Y. Yamashita and T. Yamamoto of Toshiba Medical Systems Corp., Tochigi, Japan.)

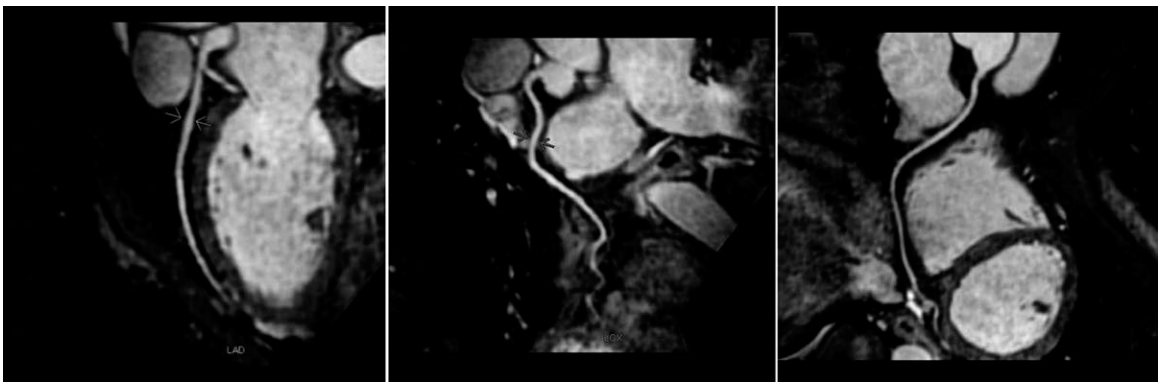

Figure 13. Example of bSSFP angiography of the coronary arteries in a 39-year-old female volunteer. Left: left anterior descending (LAD) coronary artery. Middle: left circumflex (LCX) coronary artery. Right: right coronary artery (RCA). (Image courtesy of Dr. Y. Ohmoto and staff of Radiology Department, Toranomon Hospital, Toyko, Japan.)

conventional radiology methods, indicating the potential of spin labeling NCE-MRA as a diagnostic screening test.

Flow-Out Spin Labeling Method

Description

The flow-out method applies the tagging pulse upstream on a vessel of interest (Fig. 10). The selective tagging pulse is immediately preceded by a nonselective inversion pulse (Fig. 9b). The nonselective pulse first inverts all longitudinal magnetization, including the stationary tissue and preexisting blood in the imaging slab. The tag pulse selectively restores the magnetization of the upstream tagged blood to positive longitudinal magnetization ($M_z \approx 1$) while leaving the longitudinal magnetization in the stationary tissue inverted. The process unfolds much like flow-in spin labeling; during the TI, tagged blood with full magnetization flows out of the tag region and into the imaging volume while the magnetization of stationary tissue returns toward null via T1 recovery. Like the flow-in method, the background signal is dependent on the chosen TI and stationary tissue T1.

Applications

Flow-out spin labeling has been used to depict vessels in and around the liver including hepatic arteries (76), hepatic veins (77), and the portal system (78). To depict the hepatic veins, double tag pulses were applied with one tag positioned on the upper liver to suppress signals from the aorta, and the other tag positioned below the liver to suppress signals from the portal veins (77). To depict the portal system, double tag pulses were also used (78). One tag covered the liver and thorax simultaneously to provide suppression of background signal from liver and myocardium as well as suppress inflowing blood from the hepatic arterial system. The other tag was positioned below the liver to suppress ascending venous blood signal from the inferior vena cava to avoid overlap with the signal from the portal vein. The effect of food intake on the portal system has also been studied using flow-out spin labeling (79). Another application of a 2D flow-out technique shows bulk flow movement of cerebrospinal fluid in the intracranial and intraspinal compartments (80).

Tag-Alternation Spin Labeling Method

Description

The tag-alternation method is the most standard form of spin labeling. The method can be applied in many forms, but the general concept is to acquire two scans in an alternated fashion: a tag image with upstream tagging of arterial blood and a control image without tagging (81) (Fig. 9c). The subtraction of the two image sets removes signal from stationary tissue and leaves only the tagged spins in the resultant angiogram.

The tag application can be achieved with several approaches. The tag can be applied with a selective upstream tagging pulse that is alternated on-off in the corresponding tag-control scans. This general method is used for time-SLIP (82), STAR (83), STARFIRE (84), and EPISTAR (85) techniques.

Applications

Tag-alternation spin labeling can be used for pulmonary angiography using a sagittal selective tag placed over the heart. During the TI, the blood flows out of the tag and into the lungs, where it is later read out using a 2D FSE (86) or 3D gradient-echo (87) sequence. The portal system has been studied using the tag-alternation method where both tag-on and tag-off images were acquired in a single breath-hold (88). Tag-alternation spin labeling can be used in carotid angiography with a tag applied over the heart (84). Since spin labeling NCE-MRA is not hindered by the limitations of inflow effects, it is able to depict flow in the carotid notch and bulb. An example of a time-resolved application in the left carotid artery is depicted in Figure 12.

General Considerations for Spin Labeling Methods

In the flow-in method, only blood that flows into the tag region (which corresponds to the imaging slab) is visible. This inflowing blood can come from any

Table 1
Summary of NCE-MRA Methods

Class	Method	Primary applications	Typical scan time	Vessel orientation	Stationary tissue/ venous signal background contamination
Inflow-based	3D TOF	Intracranial extracranial carotids	5 min per brain	Vessels perpendicular to slices	Moderate stationary tissue signal, Some venous (removed by segmentation)
	HOP-MRA	Intracranial	5 min per brain	Vessels perpendicular to slices	Little to none
	2D TOF	Peripheral extracranial carotids	4 min per coverage, 20 min per calf station	Vessels perpendicular to slices	Little stationary tissue signal, Some venous (removed by segmentation)
	QISS	Peripheral	1-2 min per coverage, 8-10 min iliac to calf station	Vessels perpendicular to slices	Little to none
Cardiac-phase-dependent	Cardiac-Gated 3D FSE	Pulmonary, aortic, hepatic, peripheral, extremity	3-4 min per coverage, 10-12 min liac to calf station	Vessels parallel to readout preferred	None
Flow-encoding	2D/3D PC-MRA	Flow quantification	Depends on number of PC directions	Depends on number of PC directions	No stationary tissue signal, some venous (removed by segmentation)
	4D Flow	Flow quantification, flow dynamics	10-20 min	Any	No stationary tissue signal, some venous (removed by segmentation)
	FSD	Upper and lower extremity	3-4 min per coverage	Depends on number of FSD directions	No stationary tissue signal, some venous signal
Spin labeling	Flow-In	Renal, hepatic	2 min	Any	Moderate stationary tissue signal - depends on TI
	Flow-Out	Pulmonary, CSF, carotid, hepatic	2 min	Any	Moderate stationary tissue signal - depends on TI
	Tag-Alternation	Pulmonary, carotid, CSF, extremity	3-4 min per TI increment	Any	None
Relaxation	bSSFP	Coronary, renal, extremity	14 min per whole heart volume (navigator gated, free breathing)	Any	Moderate stationary tissue signal – depends on use of T2 preparation and/or inversion recovery

supply source. In situations where an organ is fed by multiple sources, like the portal vein, which receives blood from both the splenic and the superior mesenteric veins, the relative contributions of each source vessel cannot be determined using the flow-in approach. Therefore, the flow-in method is most applicable to angiography applications. In the flow-out method, only blood selected by the finite tag region is visible. Therefore, the flow depiction can be isolated to distinct vessels. The flow-out method allows the supply functionality aspects of individual vessels to be analyzed. In the tag-alternation method, a selective tagging approach is used and hence its flow selectivity characteristics are the same as the flow-out method.

Since the flow-in method depicts inflow from any source, venous signal can also appear in the imaging slab. To further suppress venous inflow, a spatial presaturation pulse can be applied over the venous source. For example, in renal applications of flow-in spin labeling, an axial presaturation slab is commonly placed inferior to the imaging volume to suppress venous inflow from the inferior vena cava.

Although all three spin labeling methods can be used with any conventional data acquisition sequence, they usually are used with either 3D bSSFP or 3D FSE acquisition methods. Naturally, 2D acquisition is available, but like other NCE-MRA methods, the 3D acquisition is used to achieve good slice resolution. In general, the high resolution and flow-compensation of bSSFP makes it the method of choice for most applications except for pulmonary arteries and subclavian vessels near the air–tissue interface of the lungs, where FSE is preferred. Although spin-labeling techniques can be cardiac-gated if it is appropriate for the application, spin labeling does not require cardiac-gating like the cardiac-phase-dependent class of NCE-MRA methods.

The flow-in and flow-out techniques require careful selection of the TI with respect to the flow velocity in the vessel of interest and the T1 of stationary tissue. Ideally, the TI is chosen to correspond to the null point of the stationary tissue. However, if flow is slow, a longer TI might be required for good vessel depiction at the cost of increased background signal. Thus, the flow-in and flow-out techniques are best suited for applications where blood velocity is fast relative to TI. The removal of signal from stationary tissue via subtraction using the tag-alternation method avoids the dependency on TI. Therefore, the tag-alternation method can be applied for even arteries with slow-flowing blood like those in the distal extremities. Since the spin-labeling methods can be used across a range of TI, they can be used to acquire time-resolved NCE-MRA data. By incrementally adjusting TI for N repeated acquisitions, blood flow dynamics can be depicted. Since the TI can be freely selected for each of the N images, the time increment using this approach can be arbitrarily small. However, in practice, the time range and resolution is bounded by the scan time burden of N (or Nx2 in the case of tag-alternation) acquisitions. The maximum TI is bounded by the tag persistence, which decays with the T1 of tagged blood.

RELAXATION-BASED TECHNIQUES

General Mechanism of Using Relaxation for NCE-MRA

The fundamental differences in relaxation between arterial, venous, and adjacent stationary tissue can be leveraged to generate angiograms. The T2 and T2* of venous blood is shorter than that arterial blood due to the reduced oxygenation of hemoglobin (22,23). In general, the T1 of adjacent stationary tissues, whether muscles or organs, is shorter than that of blood, since blood consists of a higher percentage of free water (22). Arterial signal can be selectively depicted, and venous and stationary tissue signals relatively suppressed, using one or more approaches based on T2/T1-, T2-, T2*-, or T1-weighted contrast without the explicit removal the stationary tissue signal using saturation, subtraction, or inversion recovery mechanisms as in other NCE-MRA methods. Since the vessel depiction is independent of flow velocity, orientation, or dependency on cardiac cycle, these techniques are often referred to as "flow-independent."

The relaxation-based approach fundamentally relies on venous and surrounding stationary tissue signals decaying faster than arterial signals. Thus, these approaches result in some collateral arterial signal loss. Therefore, relaxation-based NCE-MRA must trade-off between improving the quality of suppression at the cost of arterial signal loss. In practice, signals from stationary tissue and veins are nonzero as they would be with subtraction-based methods. But depending on the application, perfect background suppression is not necessary if the vessels of interest are adequately conspicuous.

bSSFP

Technique

With the proper sequence parameter selection, the T2/T1-weighted contrast and inherent flow-compensation of bSSFP generally makes signal from stationary tissue relatively dark compared to the bright signals from the vessels. In this way, bSSFP can be used by itself as an NCE-MRA method. The bSSFP sequence depicts all blood in the imaging slab regardless of its source or flow velocity. Therefore, venous signal appears in the bSSFP images alongside arterial signal. To enhance arterial depiction, an inversion recovery pulse coupled with a T2-preparation prepulse (basically an FSD module without the flow-encoding gradients) can be used to suppress adjacent tissue and veins while leaving arterial signal mostly intact (89,90). Often, fat signal appears bright in bSSFP images. Therefore, some form of fat suppression is typically employed to increase vessel-to-background contrast.

Applications

The multidirectional flow-compensation of bSSFP makes the technique a good candidate for imaging the renal arteries. Two clinical studies comparing breath-hold bSSFP NCE-MRA with DSA (91) and CE-MRA

(92) in the detection of renal stenoses reported strong potential for bSSFP as a screening test with sensitivities of 100% and 92%, respectively, and specificities of 98% and 81%, respectively. Another clinical study reported significant improvement in image quality using respiratory navigator-gated bSSFP NCE-MRA instead of the breath-hold approach (93). The Dixon method bSSFP, where two bSSFP images acquired with different center frequency offsets are combined using the Dixon method (94), has been demonstrated to depict conspicuous vessels with good fat suppression for NCE-MRA in renal arteries (95) and arteries of the extremities (96). Also leveraging the frequency selectivity of bSSFP, fat-suppressed bSSFP NCE-MRA can be used in conjunction with an alternate TR bSSFP technique to reduce fat signal to image the arteries in the lower extremities (97).

Due to the very fast flow and lack of substantial fat or venous vasculature, bSSFP is particularly applicable to NCE-MRA in and around the heart. A common application of bSSFP is coronary NCE-MRA (98). By incorporating thin-slab 3D bSSFP with ECG-gating and breath-holding, high-resolution angiograms of the coronary arteries can be obtained (Fig. 13). More recently, free-breathing navigator-gated, whole-heart NCE-MRA has been successfully used to acquire volumetric image sets (99). The whole-heart image volume data can be repeatedly reformatted to deliver the best depiction of each vessel, which is especially useful given the curvature of the coronary arteries. Another common application of bSSFP NCE-MRA is imaging the thoracic aorta (100). The inherent flow-compensation of bSSFP is able to capture the fast arterial flow in the aorta.

SUMMARY

NCE-MRA has been demonstrated in a wide variety of cardiovascular applications including brain, heart, lungs, liver, kidneys, hands, and lower extremities. The proper NCE-MRA method for each application depends on the anatomy and characteristics of the vessels of interest. In the above discussion, established and emerging methods are compared and contrasted with regard to their features and limitations. Table 1 summarizes these techniques and their intended primary applications.

REFERENCES

1. Prince MR. Gadolinium-enhanced MR aortography. Radiology 1994;191:155–164.
2. Wilman AH, Riederer SJ, King BF, Debbins JP, Rossman PJ, Ehman RL. Fluoroscopically triggered contrast-enhanced three-dimensional MR angiography with elliptical centric view order: application to the renal arteries. Radiology 1997;205:137–146.
3. Kita M, Mitani Y, Tanihata H, et al. Moving-table reduced-dose gadolinium-enhanced three-dimensional magnetic resonance angiography: velocity-dependent method with three-phase gadolinium infusion. J Magn Reson Imaging 2001;14:319–328.
4. Ho KY, Leiner T, de Haan MW, Kessels AG, Kitslaar PJ, van Engelshoven JM. Peripheral vascular tree stenoses: evaluation with moving-bed infusion-tracking MR angiography. Radiology 1998;206:683–692.
5. Urata J, Miyazaki M, Wada H, Nakaura T, Yamashita Y, Takahashi M. Clinical evaluation of aortic diseases using nonenhanced MRA with ECG-triggered 3D half-Fourier FSE. J Magn Reson Imaging 2001;14:113–119.
6. Sadowski EA, Bennett LK, Chan MR, et al. Nephrogenic systemic fibrosis: risk factors and incidence estimation. Radiology 2007;243:148–157.
7. Roditi G, Maki JH, Oliveira G, Michaely HJ. Renovascular imaging in the NSF era. J Magn Reson Imaging 2009;30:1323–1334.
8. Moreno-Romero JA, Segura S, Mascaro JMJr, et al. Nephrogenic systemic fibrosis: a case series suggesting gadolinium as a possible aetiological factor. Br J Dermatol 2007;157:783–787.
9. Clorius S, Technau K, Watter T, et al. Nephrogenic systemic fibrosis following exposure to gadolinium-containing contrast agent. Clin Nephrol 2007;68:249–252.
10. Khurana A, Runge VM, Narayanan M, Greene JFJr, Nickel AE. Nephrogenic systemic fibrosis: a review of 6 cases temporally related to gadodiamide injection (Omniscan). Invest Radiol 2007;42:139–145.
11. Collidge TA, Thomson PC, Mark PB, et al. Gadolinium-enhanced MR imaging and nephrogenic systemic fibrosis: retrospective study of a renal replacement therapy cohort. Radiology 2007; 245:168–175.
12. Kuo PH, Kanal E, Abu-Alfa AK, Cowper SE. Gadolinium-based MR contrast agents and nephrogenic systemic fibrosis. Radiology 2007;242:647–649.
13. U.S. Food and Drug Administration. Gadolinium based contrast agents for magnetic resonance imaging (marketed as Magnevist, MultiHance, Omniscan, OptiMARK, ProHance). Rockville, MD: FDA, 2007.
14. Dawson P. Nephrogenic systemic fibrosis: possible mechanisms and imaging management strategies. J Magn Reson Imaging 2008;28:797–804.
15. Prince MR, Zhang HL, Roditi GH, Leiner T, Kucharczyk W. Risk factors for NSF: a literature review. J Magn Reson Imaging 2009;30:1298–1308.
16. Sodickson DK, Manning WJ. Simultaneous acquisition of spatial harmonics (SMASH): fast imaging with radiofrequency coil arrays. Magn Reson Med 1997;38:591–603.
17. Pruessmann KP, Weiger M, Scheidegger MB, Boesiger P. SENSE: sensitivity encoding for fast MRI. Magn Reson Med 1999;42: 952–962.
18. Miyazaki M, Lee VS. Nonenhanced MR angiography. Radiology 2008;248:20–43.
19. Morita S, Masukawa A, Suzuki K, Hirata M, Kojima S, Ueno E. Unenhanced MR angiography: techniques and clinical applications in patients with chronic kidney disease. Radiographics 2011;31:E13–E33.
20. Mizayaki M, Isoda H. Non-contrast-enhanced MR angiography of the abdomen. Eur J Radiol 2011;80:9–23.
21. Kanda T, Nakamura E, Moritani T, Yamori Y. Arterial pulse wave velocity and risk factors for peripheral vascular disease. Eur J Appl Physiol 2000;82:1–7.
22. Barth M, Moser E. Proton NMR relaxation times of human blood samples at 1.5 T and implications for functional MRI. Cell Mol Biol 1997;43:783–791.
23. Wright GA, Hu BS, Macovski A. Estimating oxygen saturation of blood in vivo with MR imaging at 1.5 T. J Magn Reson Imaging 1991;1:275–283.
24. Ono A, Murase K, Taniguchi T, et al. Deep vein thrombosis using non-contrast-enhanced MR venography with electrocardiographically-gated three-dimensional half-Fourier FSE: preliminary experience. Magn Reson Med 2009;61:907–917.
25. Masaryk TJ, Laub GA, Modic MT, Ross JS, Haacke EM. Carotid-CNS MR flow imaging. Magn Reson Med 1990;14:308–314.
26. Laub GA. Time-of-flight method of MR angiography. Magn Reson Imaging Clin N Am 1995;3:391–398.
27. Parker DL, Yuan C, Blatter DD. MR angiography by multiple thin slab 3D acquisition. Magn Reson Med 1991;17:434–451.
28. Blatter DD, Parker DL, Robinson RO. Cerebral MR angiography with multiple overlapping thin slab acquisition. Radiology 1991; 179:805–811.
29. Atkinson D, Brant-Zawadzki M, Gillan G, Purdy D, Laub G. Improved MR angiography: magnetization transfer suppression with variable flip angle excitation and increased resolution. Radiology 1994;190:890–894.
30. Pike GB, Hu BS, Glover GH, Enzmann DR. Magnetization transfer time-of-flight magnetic resonance angiography. Magn Reson Med 1992;25:372–379.

31. Edelman RR, Ahn SS, Chien D, et al. Improved time-of-flight MR angiography of the brain with magnetization transfer contrast. Radiology 1992;184:395–399.
32. Dagirmanjian A, Ross JS, Obuchowski N, et al. High resolution, magnetization transfer saturation, variable flip angle, time-of-flight MRA in the detection of intracranial vascular stenoses. J Comput Assist Tomogr 1995;19:700–706.
33. Oelerich M, Lentschig MG, Zunker P, Reimer P, Rummeny EJ, Schuierer G. Intracranial vascular stenosis and occlusion: comparison of 3D time-of-flight and 3D phase-contrast MR angiography. Neuroradiology 1998;40:567–573.
34. Korogi Y, Takahashi M, Mabuchi N, et al. Intracranial aneurysms: diagnostic accuracy of three-dimensional, Fourier transform, time-of-flight MR angiography. Radiology 1994;193:181–186.
35. White PM, Teasdale EM, Wardlaw JM, Easton V. Intracranial aneurysms: CT angiography and MR angiography for detection-prospective blinded comparison in a large patient cohort. Radiology 2001;219:739–749.
36. Willinek WA, Born M, Simon B, et al. Time-of-flight MR angiography: comparison of 3.0-T imaging and 1.5-T imaging—initial experience. Radiology 2003;229:913–920.
37. Kimura T, Ikedo M, Takemoto S. Hybrid of opposite-contrast MR angiography (HOP-MRA) combining time-of-flight and flow-sensitive black-blood contrasts. Magn Reson Med 2009;62:450–458.
38. Kimura T, Ikedo M, Takemoto S. Phase enhancement for time-of-flight and flow-sensitive black-blood MR angiography. Magn Reson Med 2011;66:437–447.
39. Tsuchiya K, Kobayashi K, Nitatori T, et al. Hybrid of opposite-contrast MRA of the brain by combining time-of-flight and black-blood sequences: initial experience in major trunk stenoocclusive diseases. J Magn Reson Imaging 2010;31:56–60.
40. Ersoy H, Zhang H, Prince MR. Peripheral MR angiography. J Cardiovasc Magn Reson 2006;8:517–528.
41. Kaufman JA, McCarter D, Geller SC, Waltman AC. Two-dimensional time-of-flight MR angiography of the lower extremities: artifacts and pitfalls. AJR Am J Roentgenol 1998;171:129–135.
42. Offerman EJ, Hodnett PA, Edelman RR, Koktzoglou I. Nonenhanced methods for lower-extremity MRA: a phantom study examining the effects of stenosis and pathologic flow waveforms at 1.5T. J Magn Reson Imaging 2011;33:401–408.
43. Heiserman JE, Drayer BP, Fram EK, et al. Carotid artery stenosis: clinical efficacy of two-dimensional time-of flight MR angiography. Radiology 1992;182:761–768.
44. Edelman RR, Sheehan JJ, Dunkle E, Schindler N, Carr J, Koktzoglou I. Quiescent-interval single-shot unenhanced magnetic resonance angiography of peripheral vascular disease: technical considerations and clinical feasibility. Magn Reson Med 2010; 63:951–958.
45. Jara H, Yu BC, Caruthers SD, et al. Voxel sensitivity function description of flow-induced signal loss in MR imaging: implications for black-blood MR angiography with turbo spin-echo sequences. Magn Reson Med 1999;41:575–590.
46. Axel L, Morton D. MR flow imaging by velocity-compensated/uncompensated difference images. J Comput Assist Tomogr 1987;11:31–34.
47. Hinks RS, Constable RT. Gradient moment nulling in fast spin echo. Magn Reson Med 1994;32:698–706.
48. Constable RT, Gore JC. The loss of small objects in variable TE imaging: implications for FSE, RARE, and EPI. Magn Reson Med 1992;28:9–24.
49. Miyazaki M, Ichinose N, Sugiura S, Kassai Y, Kanazawa H, Machida Y. A novel MR angiography technique: swap phase encode extended data (SPEED) acquisition using half-Fourier RARE. J Magn Reson Imaging 1998;8:505–507.
50. Wedeen VJ, Meuli RA, Edelman RR, et al. Projective imaging of pulsatile flow with magnetic resonance. Science 1985;230: 946–948.
51. Meuli RA, Wedeen VJ, Geller SC, et al. MR gated subtraction angiography: evaluation of lower extremities. Radiology 1986;159: 411–418.
52. Miyazaki M, Sugiura S, Tateishi F, Wada H, Kassai Y, Abe H. Non-contrast-enhanced MR angiography using 3D ECG-synchronized half-Fourier fast spin echo. J Magn Reson Imaging 2000;12:776–783.
53. Miyazaki M, Takai H, Sugiura S, Wada H, Kuwahara R, Urata J. Peripheral MR angiography: separation of arteries from veins with flow-spoiled gradient pulses in electrocardiography-triggered three-dimensional half-Fourier fast spin-echo imaging. Radiology 2003;227:890–896.
54. Nakamura K, Miyazaki M, Kuroki K, Yamamoto A, Hiramine A, Admiraal-Behloul F. Non-contrast-enhanced peripheral MRA: technical optimization of flow-spoiled fresh blood imaging for screening peripheral arterial diseases. Magn Reson Med 2011; 65:595–602.
55. Storey P, Atanasova IP, Lim RP, et al. Tailoring the flow sensitivity of fast spin-echo sequences for noncontrast peripheral MR angiography. Magn Reson Med 2010;64:1098–1108.
56. Lim RP, Hecht EM, Xu J, et al. 3D Non-gadolinium enhanced ECG-gated MRA of the distal lower extremities: preliminary clinical experience. J Magn Reson Imaging 2008;28:181–189.
57. Haneder S, Attenberger UI, Riffel P, Henzler T, Schoenberg SO, Michaely HJ. Magnetic resonance angiography (MRA) of the calf station at 3.0T: intraindividual comparison of non-enhanced ECG-gated flow-dependent MRA, continuous table movement MRA and time-resolved MRA. Eur Radiol 2011;21:1452–1461.
58. Lim RP, Storey P, Atanasova IP, et al. Three-dimensional electrocardiographically gated variable flip angle FSE imaging for MR angiography of the hands at 3.0 T: initial experience. Radiology 2009;252:874–881.
59. Dumoulin CL, Souza SP, Walker MF, Wagle W. Three-dimensional phase contrast angiography. Magn Reson Med 1989;9: 139–149.
60. Dumoulin CL, Yucel EK, Vock P, et al. Two- and three-dimensional phase contrast MR angiography of the abdomen. J Comput Assist Tomogr 1990;14:779–784.
61. Dumoulin CL. Phase contrast MR angiography techniques. Magn Reson Imaging Clin N Am 1995;3:399–411.
62. Prince MR, Schoenberg SO, Ward JS, et al. Hemodynamically significant atherosclerotic renal artery stenosis: MR angiographic features. Radiology 1997;205:128–136.
63. Iseda T, Nakano S, Miyahara D, Uchinokura S, Goya T, Wakisaka S. Poststenotic signal attenuation on 3D phase-contrast MR angiography: a useful finding in haemodynamically significant carotid artery stenosis. Neuroradiology 2000;42:868–873.
64. Markl M, Kilner PJ, Ebbers T. Comprehensive 4D velocity mapping of the heart and great vessels by cardiovascular magnetic resonance. J Cardiovasc Magn Reson 2011;13:7.
65. Markl M, Wallis W, Brendecke S, Simon J, Frydrychowicz A, Harloff A. Estimation of global aortic pulse wave velocity by flow-sensitive 4D MRI. Magn Reson Med 2010;63:1575–1582.
66. Harloff A, Nussbaumer A, Bauer S, et al. In vivo assessment of wall shear stress in the atherosclerotic aorta using flow-sensitive 3D MRI. Magn Reson Med 2010;63:1529–1536.
67. Harloff A, Simon J, Brendecke S, et al. Complex plaques in the proximal descending aorta: an underestimated embolic source of stroke. Stroke 2010;41:1145–1150.
68. Fan Z, Sheehan J, Bi X, Liu X, Carr J, Li D. 3D noncontrast MR angiography of the distal lower extremities using flow-sensitive dephasing (FSD)-prepared balanced SSFP. Magn Reson Med 2009;62:1523–1532.
69. Fan Z, Zhou X, Bi X, Dharmakumar R, Carr J, Li D. Determination of optimal first-order gradient moment for flow-sensitive dephasing magnetization-prepared 3D noncontrast MR angiography. Magn Reson Med 2011;65:964–972.
70. Sheehan JJ, Fan Z, Davarpanah AH, et al. Nonenhanced MR angiography of the hand with flow-sensitive dephasing-prepared balanced SSFP sequence: initial experience with systemic sclerosis. Radiology 2011;259:248–256.
71. Priest AN, Graves MJ, Lomas DJ. Non-contrast-enhanced vascular magnetic resonance imaging using flow-dependent preparation with subtraction. Magn Reson Med 2012;67:628–637.
72. Spuentrup E, Manning WJ, Bornert P, Kissinger KV, Botnar RM, Stuber M. Renal arteries: navigator-gated balanced fast field-echo projection MRA with aortic spin labeling: initial experience. Radiology 2002;225:589–596.
73. Wyttenbach R, Braghetti A, Wyss M, et al. Renal artery assessment with nonenhanced steady-state free precession versus contrast-enhanced MR angiography. Radiology 2007;245:186–195.
74. Lanzman RS, Voiculescu A, Walther C, et al. ECG-gated nonenhanced 3D steady-state free precession MR angiography in assessment of transplant renal arteries: comparison with DSA. Radiology 2009;252:914–21.
75. Parienty I, Rostoker G, Jouniaux F, Piotin M, Admiraal-Behloul F, Miyazaki M. Renal artery stenosis evaluation in chronic

kidney disease patients: nonenhanced time-spatial labeling inversion-pulse three-dimensional MR angiography with regulated breathing versus DSA. Radiology 2011;259:592–601.
76. Shimada K, Isoda H, Okada T, et al. Non-contrast-enhanced hepatic MRA with true steady-state free-precession and time spatial labeling inversion pulse: optimization of the technique and preliminary results. Eur J Radiol 2009;70:111–117.
77. Shimada K, Isoda H, Okada T, et al. Non-contrast-enhanced MRA for selective visualization of the hepatic vein and inferior vena cava with true steady-state free-precession sequence and time-spatial labeling inversion pulses: preliminary results. J Magn Reson Imaging 2009;29:474–479.
78. Shimada K, Isoda H, Okada T, et al. Non-contrast-enhanced MR portography with time-spatial labeling inversion pulses: comparison of imaging with three-dimensional half-Fourier fast spin-echo and true steady-state free-precession sequences. J Magn Reson Imaging 2009;29:1140–1146.
79. Tsukuda T, Ito K, Koike S, Sasaki et al. Pre- and postprandial alterations of portal venous flow: evaluation with single breath-hold three-dimensional half-Fourier fast spin-echo MR imaging and a selective inversion recovery tagging pulse. J Magn Reson Imaging 2005;22:527–533.
80. Yamada S, Miyazaki M, Kanazawa H, et al. MRI visualization of cerebrospinal fluid movement with spin labeling: preliminary results in normal and pathophysiological conditions. Radiology 2008;249:644–652.
81. Nishimura DG, Macovski A, Pauly JM, Conolly SM. MR angiography by selective inversion recovery. Magn Reson Med 1987;4: 193–202.
82. Kanazawa H, Miyazaki M.Time-spatial labeling inversion tag (t-SLIT) using a selective IR-tag on/off pulse in 2D and 3D half-Fourier FSE as arterial spin labeling. In: Proc 10th Annual Meeting ISMRM, Honolulu; 2002. p140.
83. Edelman RR, Siewert B, Adamis M, Gaa J, Laub G, Wielopolski P. Signal targeting with alternating radiofrequency (STAR) sequences: application to MR angiography. Magn Reson Med 1994;31:233–238.
84. Koktzoglou I, Edelman RR. Star and STARFIRE for flow-dependent and flow-independent noncontrast carotid angiography. Magn Reson Med 2009;61:117–124.
85. Edelman RR, Chen Q. EPISTAR MRI: multislice mapping of cerebral blood flow. Magn Reson Med 1998;40:800–805.
86. Mai VM, Berr SS. MR perfusion imaging of pulmonary parenchyma using pulsed arterial spin labeling techniques: FAIRER and FAIR. J Magn Reson Imaging 1999;9:483–487.
87. Mai VM, Hagspiel KD, Altes T, Goode AR, Williams MB, Berr SS. Detection of regional pulmonary perfusion deficit of the occluded lung using arterial spin labeling in magnetic resonance imaging. J Magn Reson Imaging 2000;11:97–102.
88. Ito K, Shimizu A, Tsukada T, et al. Evaluation of intraportal venous flow distribution by unenhanced MR angiography using three-dimensional fast spin-echo with a selective tagging pulse: efficacy of subtraction of tag-on and tag-off images acquired during a single breath-hold. J Magn Reson Imaging 2009;29: 1224–1229.
89. Brittain JH, Hu BS, Wright GA, Meyer CH, Macovski A, Nishimura DG. Coronary angiography with magnetization-prepared T2 contrast. Magn Reson Med 1995;33:689–696.
90. Shea SM, Deshpande VS, Chung YC, Li D. Three-dimensional true-FISP imaging of the coronary arteries: improved contrast with T2-preparation. J Magn Reson Imaging 2002;15:597–602.
91. Coenegrachts K, Hoogeveen R, Vaninbroukx J, et al. High-spatial resolution 3D balanced turbo field-echo technique for MR angiography of the renal arteries: initial experience. Radiology 2004;231:237–242.
92. Herborn C, Watkins D, Runge V, Gendron J, Montgomery M, Naul L. Renal arteries: comparison of steady-state free precession MR angiography and contrast-enhanced MR angiography. Radiology 2006;239:263–268.
93. Maki JH, Wilson GJ, Eubank WB, Glickerman DJ, Pipavath S, Hoogeveen RM. Steady-state free precession MRA of the renal arteries: breath-hold and navigator-gated techniques vs. CE-MRA. J Magn Reson Imaging 2007;26:966–973.
94. Huang TY, Chung HW, Wang FN, Ko CW, Chen CY. Fat and water separation in balanced steady-state free precession using the Dixon method. Magn Reson Med 2004;51:243–247.
95. Stafford RB, Sabati M, Haakstad MJ, Mahallati H, Frayne R. Unenhanced MR angiography of the renal arteries with balanced steady-state free precession Dixon method. Am J Roentgenol 2008;191:243–246.
96. Stafford RB, Sabati M, Mahallati H, Frayne R. 3D non-contrast enhanced MR angiography with balanced steady-state free precession Dixon method. Magn Reson Med 2008;59:430–433.
97. Çukur T, Lee JH, Bangerter NK, Hargreaves BA, Nishimura DG. Non-contrast-enhanced flow-independent peripheral MR angiography with balanced SSFP. Magn Reson Med 2009;61: 1533–1539.
98. Deshpande VS, Shea SM, Laub G, Simonetti OP, Finn JP, Li D. 3D magnetization-prepared true-FISP: a new technique for imaging coronary arteries. Magn Reson Med 2001;46:494–502.
99. Sakuma H, Ichikawa Y, Suzawa N, et al. Assessment of coronary arteries with total study time of less than 30 minutes by using whole-heart coronary MR angiography. Radiology 2005;237: 316–321.
100. Amano Y, Takahama K, Kumita S. Non-contrast-enhanced MR angiography of the thoracic aorta using cardiac and navigator-gated magnetization-prepared three-dimensional steady-state free precession J Magn Reson Imaging 2008;27:504–509.